JGR Space Physics

RESEARCH ARTICLE
10.1029/2023JA031813

**Key Points:**

- SuperMAG ultra-low frequency (ULF) parameters are used to study the spatial and temporal responses of ULF waves to pressure impulses
- The ULF power has great differences in the distribution as a function of magnetic local time and L-shell
- Seasonal effects have significant influences on the magnetic field power in different bands

**Supporting Information:**

Supporting Information may be found in the online version of this article.

**Correspondence to:**

Q. G. Zong and J. Ren,
qgzong@pku.edu.cn;
renjiepkusdu@gmail.com

**Citation:**

Xie, Z.-K., Zong, Q. G., Ren, J., Yue, C., Liu, Z.-Y., Liu, J.-J., et al. (2023). Global ULF waves excited by solar wind dynamic pressure impulses: 1. timescales and geomagnetic activity dependence. *Journal of Geophysical Research: Space Physics*, *128*, e2023JA031813. https://doi.org/10.1029/2023JA031813

Received 28 JUN 2023
Accepted 6 OCT 2023



# Global ULF Waves Excited by Solar Wind Dynamic Pressure Impulses: 1. Timescales and Geomagnetic Activity Dependence

**Zi-Kang Xie[1], Q. G. Zong[1,2], Jie Ren[1], Chao Yue[1], Zhi-Yang Liu[1], Jian-Jun Liu[3], Ze-Jun Hu[3], Xing-Yu Li[1], Ze-Fan Yin[1], Yun Yan[1], Li Li[1], and J. W. Gjerloev[4]**

[1]Institute of Space Physics and Applied Technology, Peking University, Beijing, China, [2]State Key Laboratory of Lunar and Planetary Sciences, Macau University of Science and Technology, Taipa, Macau, China, [3]MNR Key Laboratory for Polar Science, Polar Research Institute of China, Shanghai, China, [4]Department of Physics and Technology, University of Bergen, Bergen, Norway

**Abstract** Solar wind dynamic pressure pulse is one of the sources of ultra-low frequency (ULF) waves. Based on 1-second resolution magnetic field observations from SuperMAG from 2012 to 2019, we conducted a statistical study on temporal and spatial variations of global ULF power after the arrival of positive dynamic pressure pulses. The magnetosphere responds quickly to the dynamic pressure pulse within 1 min. At low L-shells, it takes 4–6 min for the ULF waves to reach a power maximum, then ULF waves decay on a timescale of about 10 min. The spatial distribution of ULF wave power is closely related to the direction of the interplanetary magnetic field (IMF) when the dynamic pressure pulse arrives. The southward IMF leads to the reconnection on the dayside and more intense substorm activities on the nightside, accompanied by stronger ULF wave power globally. The power enhancement in the Pc2 band exhibits a notable fluctuation concentrated primarily in the range of $L = 7$ to 9, compared with the quiet period. In contrast, the amplification of Pc3 wave power occurs predominantly at higher L-shells. However, the fluctuation of Pc5 power exhibits an opposite pattern, indicating disparate excitation and propagation mechanisms. In addition, seasonal effects affect the ULF power in different bands, which can be explained by the Russell-McPherron (R-M) effect. Our statistical results on long-term, global-scale geomagnetic observations illustrate that pressure pulses are important sources of ULF waves, and the spatial distribution of wave power varies greatly under different solar wind conditions.

## 1. Introduction

Geomagnetic activity has been studied for over a century. As a widespread geomagnetic phenomenon, geomagnetic pulsations (also known as ULF waves) are thought to be driven by the solar wind and the interplanetary magnetic field (IMF). These pulsations can be divided into two main classes: Pc and Pi, which represent continuous and irregular fluctuations, respectively (Jacobs et al., 1964). The mechanisms of excitation and propagation of fluctuations at different frequencies vary considerably.

The two energy sources for ULF waves are the solar wind outside the magnetosphere and the instability inside the magnetosphere. The shock with a positive pressure pulse compresses the magnetopause and causes the disturbance of the geomagnetic signals, which is known as "storm sudden commencement" (SSC), first observed in the 1940s (Chapman & Bartels, 1940; Hao et al., 2019). The interaction between solar wind dynamic pressure pulses and the magnetosphere has been widely investigated in previous studies, which suggest these pulses serve as possible sources of ULF waves (Engebretson et al., 2015; Tan et al., 2004; Yang et al., 2008; C. Yue et al., 2010, 2011; Zong et al., 2012, 2009, 2017; X. Zhang et al., 2009). ULF waves excited by IP shock impact or solar wind positive and negative dynamic pressure pulses (X. Y. Zhang et al., 2010) exhibit rapid decay. Strong Alfvén waves with a period of approximately 100–150 s that decay within 15 min near the plasmaspheric boundary layer, are observed by the Cluster spacecraft (Zong et al., 2009). Li et al. (2003) proposed that the propagation speed of the electric field impulse induced by the IP shock is approximately 1,200 km/s. The propagation speed of the wavefront induced by the IP shock in the outer magnetosphere has been measured to be 1249.7 km/s (Zong et al., 2009). These findings collectively suggest that the interaction timescale between the IP shock and the magnetosphere is approximately 1 minute (Z. Y. Liu et al., 2017). For the response of ground and low-Earth orbit (LEO) magnetic fields, Vassiliadis et al. (2007) studied the growth and decay characteristics of Pc3-Pc5 wave power as well as its distribution as a function of $L$ shell in response to the solar wind velocity $V$sw. They found

that the ground ULF wave power is structured and uniformly distributed in the range of $L = 3.5$ to 6.4 and $L = 6.4$ to 15, respectively. The response of wave power to *V*sw is characterized by an increase in the hours before the peak and a rapid decline in the following 2 days. The response and spatial distribution of ULF waves differ greatly for dynamic pressure pulses under different IMF conditions.

Pc1-2 waves (periods ∼0.2–10 s) originate mainly from electromagnetic ion cyclotron (EMIC) instability within the magnetosphere (Allen et al., 2015; Anderson et al., 1992; Z. Y. Liu et al., 2022; Min et al., 2012). Engebretson et al. (2015) analyzed an EMIC wave event excited by a sharp increase in solar wind dynamic pressure based on spacecraft and ground observations. The enhancement of the solar wind dynamic pressure leads to an increase in the ion temperature anisotropy and further excites the EMIC waves in the Pc1-2 band (Anderson & Hamilton, 1993; Jun et al., 2021; Usanova et al., 2008; C. Yue et al., 2011, 2016).

Multiple spacecraft observation analyses have been done to study the spatial distribution of Pc3-5 ULF waves. Anderson et al. (1990) used Active Magnetospheric Particle Tracers Explorers Charge Composition Explorer (AMPTE/CCE, Potemra et al. (1985)) magnetic field observations to obtain the spatial distributions of Pc5 ULF waves with respect to L-shell and the MLT. They found that the harmonic toroidal resonances mainly occurred on the dayside, and during the storm time, Pc5 waves are often observed at duskside. Using 4 years of AMPTE/CCE data, Takahashi and Anderson (1992) draw the spatial distribution of ULF power and find that the equatorial compressional Pc3 oscillations mainly occur in the prenoon sector between $L = 3$ to $L = 5$. Based on 10 years of magnetometer array data, Baker et al. (2003) found that Pc5 pulsations mainly appeared in the dawn and dusk sectors, and the occurrence rate in the dawn side is higher than that in the duskside. W. Liu et al. (2009) get the spatial distribution of Pc4 to Pc5 waves covering all MLTs by using 13-month magnetic field and electric field measurements of Time History of Events and Macroscale Interactions During Substorms (THEMIS, Angelopoulos (2008)). Their statistical results show that Pc4 wave events often occur around 5–6 Re. In the noon sector, the power of Pc5 ULF waves is dominated by the poloidal mode. The distribution of ULF wave power is significantly related to the Kp index. Previous studies have used Combined Release and Radiation Effects Satellite (Ali et al., 2015), THEMIS satellite (W. Liu et al., 2016) and Van Allen Probes (Ali et al., 2016) to calculate the electric and magnetic field diffusion coefficients of ULF waves. These statistical results show the same characteristics, that is, the power of ULF waves in the outer magnetosphere is stronger, and the power of ULF waves at lower L-shell increases with the intensity of geomagnetic activities.

Although the spatial distribution of ULF waves and their excitation mechanisms have been studied for decades using observations from magnetospheric satellites, there is a lack of long-term, global statistical studies on ground ULF wave power after the arrival of the dynamic pressure pulses. In this study, we aim to examine the integrated ULF wave power of ground stations to investigate the global response of ULF waves to positive pulses of solar wind dynamic pressure under different IMF conditions. Section 2 describes the data set of ULF parameters, the identification of dynamic pressure pulses, and statistical methods for wave power. Section 3.1 delves into a detailed analysis of ULF power distributions in terms of L-shell and MLT, followed by a statistical analysis of the relationship between ULF fluctuations and geomagnetism, substorm activity, and dynamic pressure pulse intensity. In Section 3.2, we scrutinize the behavior of ULF waves triggered by dynamic pressure pulses at varying L-shells. Section 3.3 focuses on the nature of statistically longer-term ULF fluctuations, including seasonal and annual variations. Finally, in Sections 4 and 5, we discuss and summarize the principal findings of our investigation.

## 2. Data Set and Methods

### 2.1. Data Set

In this study, we use the 1-second resolution ULF parameters derived from ground magnetometer measurements given by SuperMAG based on the measurements of geomagnetic stations (Gjerloev, 2012). The ULF parameters are derived from the SuperMAG 1-s data by the wavelet transform. For the SuperMAG 1-s data, the main field, or baseline, has been removed using the technique described in Gjerloev (2012), to subtract the daily variations and yearly trends. Figure S1 shows the original data of the geomagnetic field measurements, the SuperMAG 1-s data, where the baseline has been removed, and the wavelet spectrum of the SuperMAG 1-s data. The detailed calculation method of the ULF parameters is provided on the SuperMAG website (https://supermag.jhuapl.edu/info/data.php?page=ulf). The WIND observation is used to identify events with positive dynamic pressure

pulses. To derive the solar wind dynamic pressure $p_{dyn} = n_{sw} m_i v_{sw}^2$ ($n_{sw}$ is the proton number density, $m_i$ is proton mass, and $v_{sw}$ is the solar wind velocity), we use the high-resolution (3 s) data from 3-D Plasma and Energetic Particle Investigation (3DP) instrument onboard the WIND spacecraft (Lepping et al., 1995; Lin et al., 1995). The one-minute resolution solar wind parameters (including IMF, solar wind velocity and dynamic pressure) and global geomagnetic parameters are obtained from the OMNI database (King & Papitashvili, 2005). The SYM-H index is used to determine the arrival time of dynamic pressure pulses, as described in Y. Liu and Zong (2015). For the statistical study, we use the list of Wind IP shocks obtained from the Harvard Smithsonian Center for Astrophysics Interplanetary Shock Database (https://www.cfa.harvard.edu/shocks/wi_data/).

### 2.2. The Positive Dynamic Pressure Pulses

From 2012 to 2019, the 176 positive dynamic pressure pulse events we find come from two parts. The first part comes from the CFA Interplanetary Shock Database, including 112 forward and NN type shocks with dynamic pressure enhancement. The second part of events is identified by an algorithm:

1. Search for time points that satisfy $\Delta\text{Pressure}/\Delta t > 0.01$ nPa/s.
2. Group these time points. The gap between the end time of the previous group and the start time of the next group is greater than 1 hr. The start time of each group is recorded as $t_0$.
3. Calculate the standard deviation $\text{STD}_0$ of the pressure in [$t_0$−6,000 s, $t_0$−500 s].
4. Search for the time $t_{start}$ that first satisfies $\Delta\text{Pressure} < 2\text{STD}_0$ in [$t_0$−2,000 s, $t_0$]. The time interval of ΔPressure is 100 s. $t_{start}$ is the start time of the candidate dynamic pressure pulse. If it is not found, continue the search.
5. Perform artificial screening to exclude events with turbulent pressure.

### 2.3. Responses of the Ground Magnetic Field

As mentioned in the Introduction section, the IP shock can compress the magnetopause, which increases the power of the ULF waves. Figure 1 shows examples of such power enhancement on 22 June 2015. The red dotted line marks the arrival time of the shock. At about 18:33 UT, a positive solar wind dynamic pressure impulse was observed. The SYM-H index increases from ∼−20–88 nT in 2 min, standing for the IP pulse arrival. The solar wind dynamic pressure enhances from 5 to 50 nPa, the proton number density jumps from around 10 to 60 $cm^{-3}$ and the solar wind speed increases from 440 to 640 km/s. The solar wind impulse simultaneously excites ULF waves and the enhancement of integrated ULF power in various bands has been observed by geomagnetic stations at different latitudes as shown in Figures 1a2–1h2. As shown in Figure 2, we can see a significant increase in global Pc3-5 ULF wave power after the arrival of the shock.

### 2.4. Statistics

In this paper, we use superposed epoch analysis to study the different responses of ULF waves to the positive solar wind dynamic pressure impulses for all identified cases. The zero-epoch time is chosen as the arrival time of the pressure impulses.

The statistical results are the distribution of ULF power as the function of ($t$, $L$, MLT), where $t$ is the epoch time, $L$ is the L-shell parameter calculated from the international reference geomagnetic field (IGRF) model, MLT is the MLT. To obtain the distributions as a function of ($t$, $L$, MLT), we first divide the L-shell from 1 to 12 into 11 bins, the MLT into 24 bins, and calculate the median values and the data numbers of each bin. Then we apply the weighted median values in time to get one-minute resolution data. Finally, we calculate the weighted median values over 173 events and obtain power distributions as a function of ($t$, $L$, MLT).

## 3. Results

### 3.1. ULF Power Distributions in the L-MLT Plane

Figure 3 shows the power distribution within 0.2 hr after pressure pulse arrival in the L-MLT plane under different IMF conditions. Among all 173 events, there are 86 and 87 events satisfying IMF Bz < 0 and Bz > 0, respectively.

As shown in Figures 3a1–3c1, Pc2 wave power is significantly stronger around $L = 9$ in the post-noon region, and the dayside power is stronger than the nightside power. Pressure pulses can cause an increase in the temperature

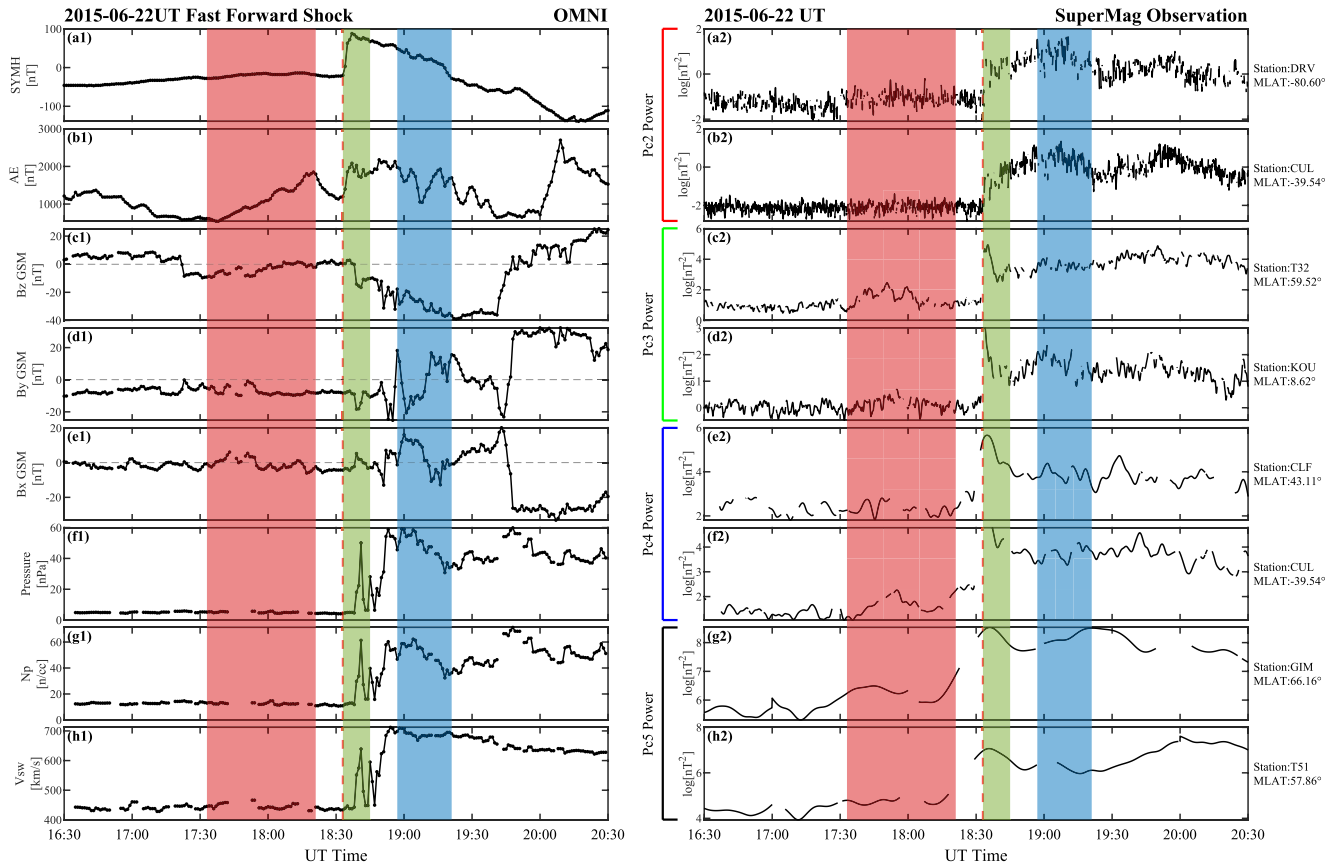


**Figure 1.** An example of the ultra-low frequency power enhancement during the IP shock on 22 June 2015. (a1) Symmetric-H index. (b1) AE index. (c1–e1) The geocentric solar magnetospheric (GSM) coordinate x, y and z components of interplanetary magnetic field (IMF). (f1–h1) The solar wind dynamic pressure, proton number density and solar wind speed. (a2–b2), (c2–d2), (e2–f2), and (g2–h2) show the magnetic field power of Pc2, Pc3, Pc4, and Pc5 waves observed from different stations, respectively. In panels (a–h), three rectangles marked in red, green and blue represent the time periods before the shock, just after the shock arrives, and after the shock arrival, respectively.

anisotropy of the ring current ions in the dayside magnetosphere, thus providing a free energy source for Pc2 wave excitation outside the plasmasphere. During active geomagnetic conditions, injected hot ions which drift westward near the Earth, may reach plasmaspheric plumes, causing intense EMIC waves in the postnoon to dusk sector (Anderson et al., 1992; Yan, Yue, Ma, et al., 2023; Yan, Yue, Yin, et al., 2023). Compared with the northward IMF, the Pc2 wave power in the pre-night sector is enhanced when the IMF is southward. These features are consistent with previous observation of EMIC waves (Min et al., 2012). When IMF Bz $< 0$, it can trigger magnetic reconnection events at the dayside magnetopause. These reconnection events can release stored energy in the Earth's magnetosphere, which can lead to the injection of energetic particles into the magnetosphere. These substorm injected particles can in turn enhance the growth of EMIC waves on the nightside of the Earth.

The region with strong Pc3 wave power covers a wide L-shell range, mainly concentrated in the region from post-noon to dawn, as shown in Figures 3a2–3c2. This phenomenon suggests the existence of a source region of Pc3 fluctuations in the dayside magnetopause. The peak amplitude locates at the pre-noon region. Greenstadt and Russell (1994) pointed out that the pre-noon quasi-parallel shock region is the place where Pc3 waves are generated.

The distributions of Pc4 and Pc5 waves are more uniform on MLT. Even so, we can still see a significant increase in wave power on the dayside. During the solar wind pressure impulse, the compression and expansion of the Earth's magnetosphere can generate fast-mode waves which can propagate across the field lines, couple with the Alfvén waves and cause the field line resonance. These waves can travel from the dayside magnetopause, where the solar wind interacts with the Earth's magnetosphere, to the dayside ionosphere, where these waves can be observed as ground-based ULF waves. For the power enhancement on the nightside during the southward

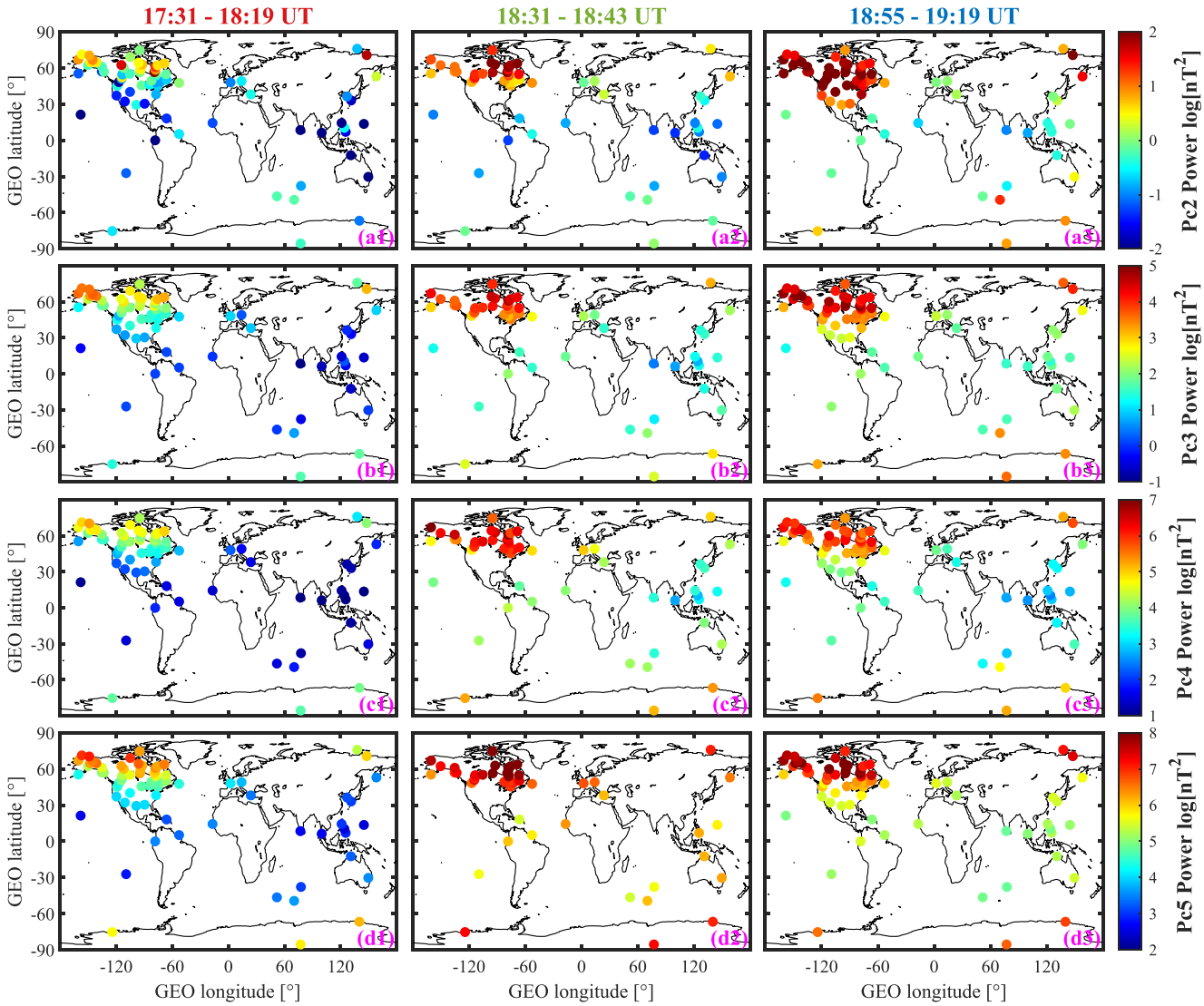


**Figure 2.** The variation of ultra-low frequency power for different Pc bands as a function of geographic locations during different time periods measured by SuperMAG stations. (a1–d1), (a2–d2), (a3–d3) respectively represent the time period before the shock, just after the shock arrives, and after the shock arrival marked in Figure 1. (a–d) Show the magnetic field power of Pc2, Pc3, Pc4, and Pc5 waves observed from different stations.

IMF, the main mechanism is related to the enhanced substorm activity (Figure 4). Plasma and energy enter the magnetosphere during reconnection, leading to the triggering of substorms during which energetic particles can be injected into the inner magnetosphere from the plasma sheet on the nightside. Then the injected particles can excite ULF waves through wave-particle interactions such as drift resonance (Hao et al., 2014) and drift-bounce resonance (Z. Y. Liu et al., 2020; Ren et al., 2015). It is worth noting that for the region from $L = 6$ to $L = 9$, the Pc5 fluctuations during quiet periods exhibit the same characteristics as those reported by Baker et al. (2003), with stronger wave power on the dawn-dusk side and weaker power in the noon sector. However, this phenomenon is no longer observed after the arrival of the dynamic pressure pulses. Based on these results, we believe that the Pc5 fluctuations during quiet periods are mainly caused by the Kelvin-Helmholtz (K-H) instability on the dawn-dusk sides, while dynamic pressure pulses can enhance the Pc5 fluctuations near the noon.

In general, after the arrival of the pulses, the dayside wave power is stronger than the nightside, and this trend becomes weaker as the frequency decreases. In other words, the longer the wavelength, the more uniform the distribution of power in the MLT. When the IMF is dominantly southward, the power increases globally. Approximately, the power of the pre-night region can get greater enhancements. In contrast to Bz < 0, no significant enhancement is found in the night region when the IMF is dominantly northward.

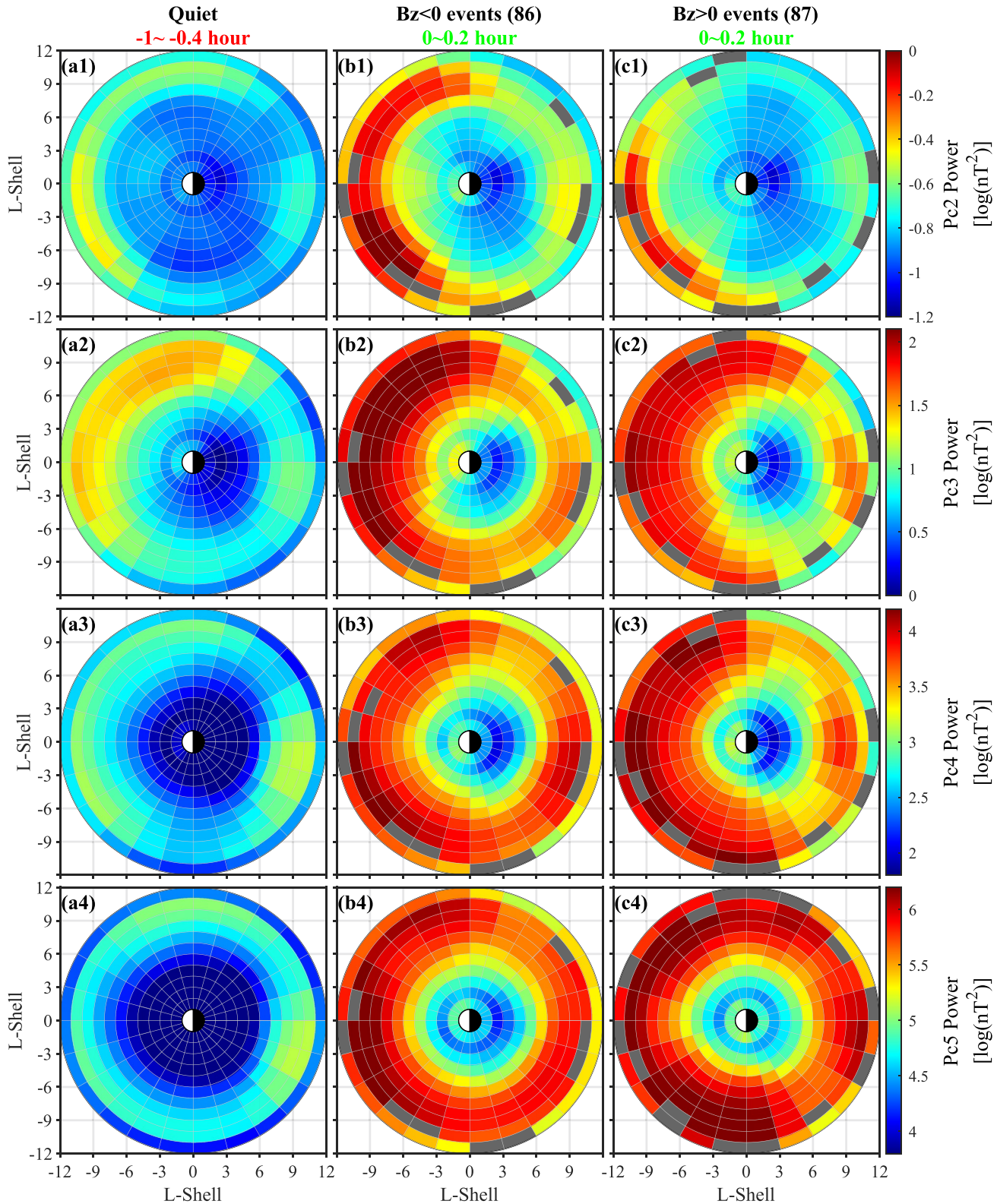


**Figure 3.** Superposed epoch analysis of power distributions in the L-MLT plane under different IMF conditions. (a) Quiet time distributions, the corresponding time range is −1∼−0.4 hr (b, c) The distributions under the conditions of IMF Bz < 0 and Bz > 0, the corresponding epoch time range is 0 ∼ 0.2 hr after the pulse arrival.

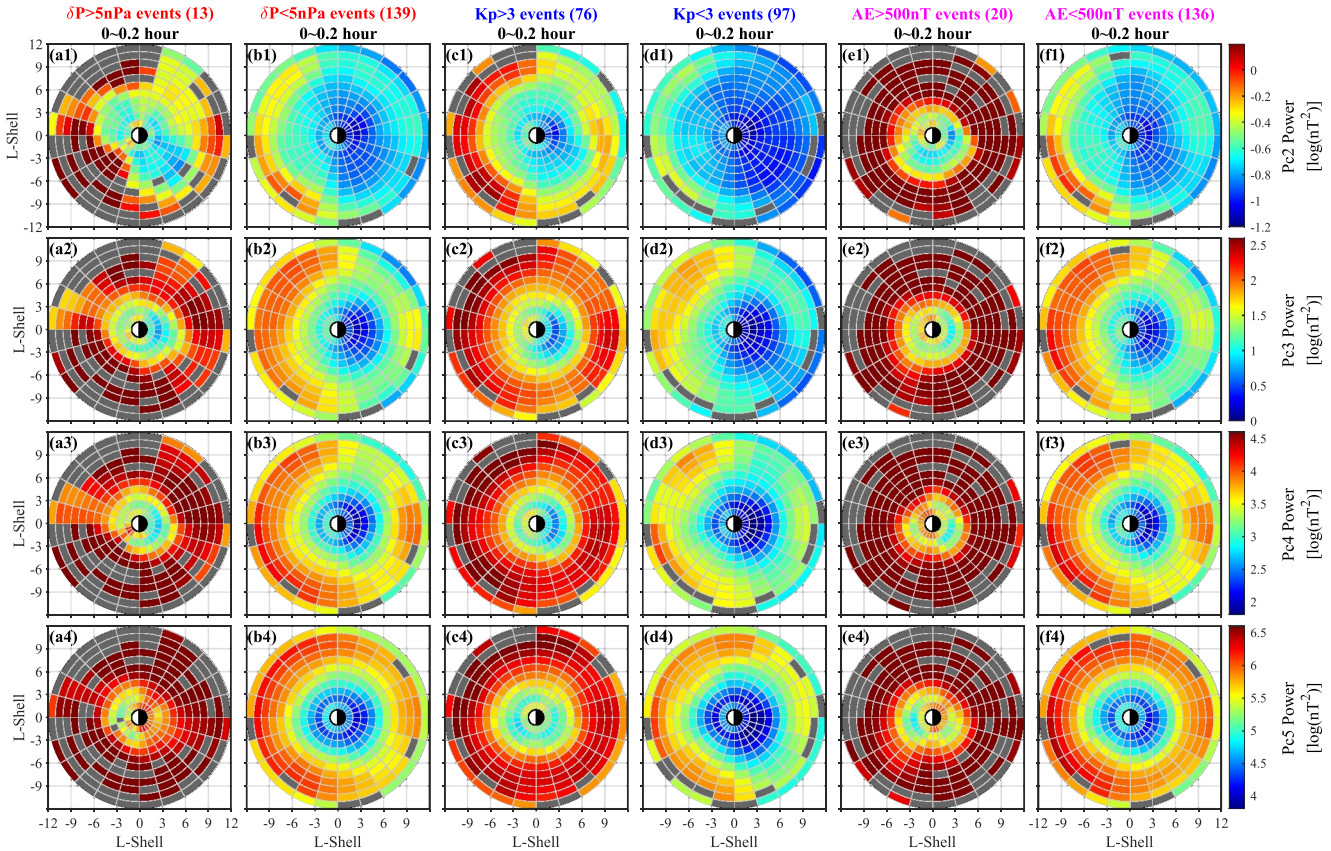


**Figure 4.** Superposed epoch analysis of power distributions in the L-MLT plane under different dynamic pressure pulse intensities and geomagnetic conditions (Kp index and AE index). (a, b) The spatial distribution of ultra-low frequency waves under different pulse amplitudes of the dynamic pressure. There are 13 events that satisfy $\delta P > 5$ nPa in 100 s (c, d) Spatial distributions under different intensities of Kp index. There are 76 events that satisfy Kp > 3. (e, f) Spatial distributions with different substorm intensities. There are 20 events that satisfy AE > 500 nT.

Furthermore, it is necessary to figure out the association between magnetospheric ULF wave activities and dynamic pressure pulse intensity. The results indicate that stronger dynamic pressure pulses indeed generate stronger ULF power. Panels (a1–a4) and panels (b1–b4) of Figure 4 illustrate the ULF power distributions triggered by strong and weak amplitude dynamic pressure pulses, respectively, with a threshold of $\delta P = 5$ nPa within 100 s. Interestingly, it is worth noting that ULF waves triggered by larger dynamic pressure pulses are more active on the nightside. This indicates that there is an effective energy transfer from the dayside to the nightside, and that the carrier of this process may be the fluctuation of various frequency bands. These fluctuations unload the free energy brought by the enhanced dynamic pressure on the dayside to the nightside, resulting in an increase in wave power in wide frequency bands. This, in turn, causes the particles on the nightside to be further heated and accelerated.

ULF power has different dependence characteristics on different geomagnetic indices. As shown in Figures 4c1–4d4, a higher Kp index is accompanied by more intense global ULF waves. Similarly, as shown in Figures 4e1–4f4, when the substorm activity accompanied by the dynamic pressure pulse is more intense, the ULF fluctuation intensity on the nightside can reach the same magnitude as that on the dayside. This result suggests that strong substorm injection accompanied by dynamic pressure pulses is also an important energy source of ULF waves.

### 3.2. ULF Power Distributions as a Function of L-Shell

Figures 5a–5d show the superposed epoch results of the SYM-H index, the AE index, solar wind pressure and IMF Bz, respectively. It is clear that the SYM-H index presents obvious enhancement at first and then drops slowly after the pulse arrival. Compared with the SYM-H index, AE index also increases. When the southward

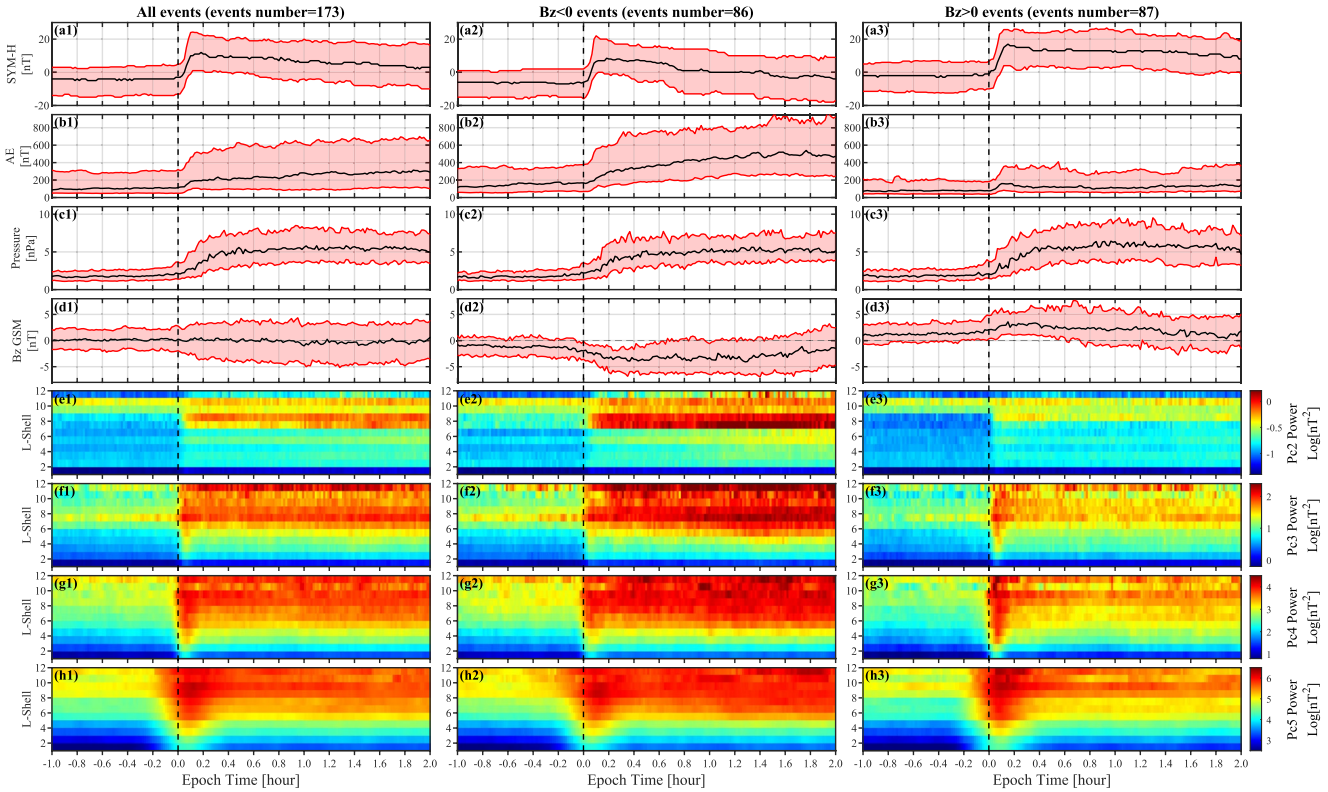


**Figure 5.** Superposed epoch analysis of power distributions as a function of L-shell under different IMF conditions. The 4 panels on the top are (a) SYM-H index, (b) AE index, (c) OMNI dynamic pressure and (d) IMF Bz in GSM coordinate. The black lines represent the median values, and the top and bottom red lines are the upper and lower quartiles, respectively. (e–h) Power distributions as a function of epoch time and L-Shell from Pc2 to Pc5 bands, respectively. From left column to right column, the IMF conditions and the corresponding number of events are marked on the top of (a1–a3), respectively.

IMF dominates, the AE index is larger than that of the northward IMF. This might be related to the magnetic reconnection triggered by the southward IMF with stronger substorm activities.

In the quiet period, the peak amplitude of Pc2 wave power is mainly centered at $L = 9 \sim 11$. As shown in Figures 5e1–5e3, immediately following the pressure pulse arrival, Pc2 wave power enhances in all L-shells. As shown in Figures 5e1–5e3, the strongest enhancement region is around $L = 8$. For $L > 10$, there is a significant enhancement with Bz < 0, but the wave power is basically maintained at the level of the quiet state when IMF is northward. The location of Pc2 peak power extends to around L ~ 7 with southward IMF. However, this phenomenon is not significant in the northward IMF condition. Because the Pc2 band is within the frequency range of the EMIC waves, and we find that the AE index is larger with southward IMF. We believe that the substorm activity accompanied with ion implantation and the ion anisotropy enhancement leads to stronger Pc2 fluctuations.

For the Pc3 and Pc4 wave power with northward IMF shown in Figures 5f3–5g3, the time when the power reaches maximum depends on the L-shell. In the $L > 6$ region, the power increases to the maximum value on a time scale of around 1 min, but it takes $4 \sim 5$ min for the region of $L < 5$. During the power unloading stage, the power dissipation is faster in the lower $L$ region, and it takes about 8 min to reach the average power level after the arrival of pulses. However, for the southward IMF cases shown in Figures 5f2–5g2, the power increases and maintains simultaneously in the overall L-shell regions.

As shown in Figures 5h1–5h3, for long-period Pc5 fluctuations, in the stage of the power enhancement, the larger the L-shell is, the earlier the maximum wave power will be reached. Whether the IMF is northward or southward, the time scale required for the power to reach its maximum at all L-shells is about 10 min and it takes about 15 min to decay. Hao et al. (2017) present a case study of shock-induced Pc5 waves, and the decay time scale is about 10 min. Our statistical results show the same characteristic time scale.

To compare the power distribution characteristics of different L-shells more quantitatively, it is necessary to use a more rigorous approach. Figure 6 illustrates the ratio of the power after the arrival of dynamic pressure

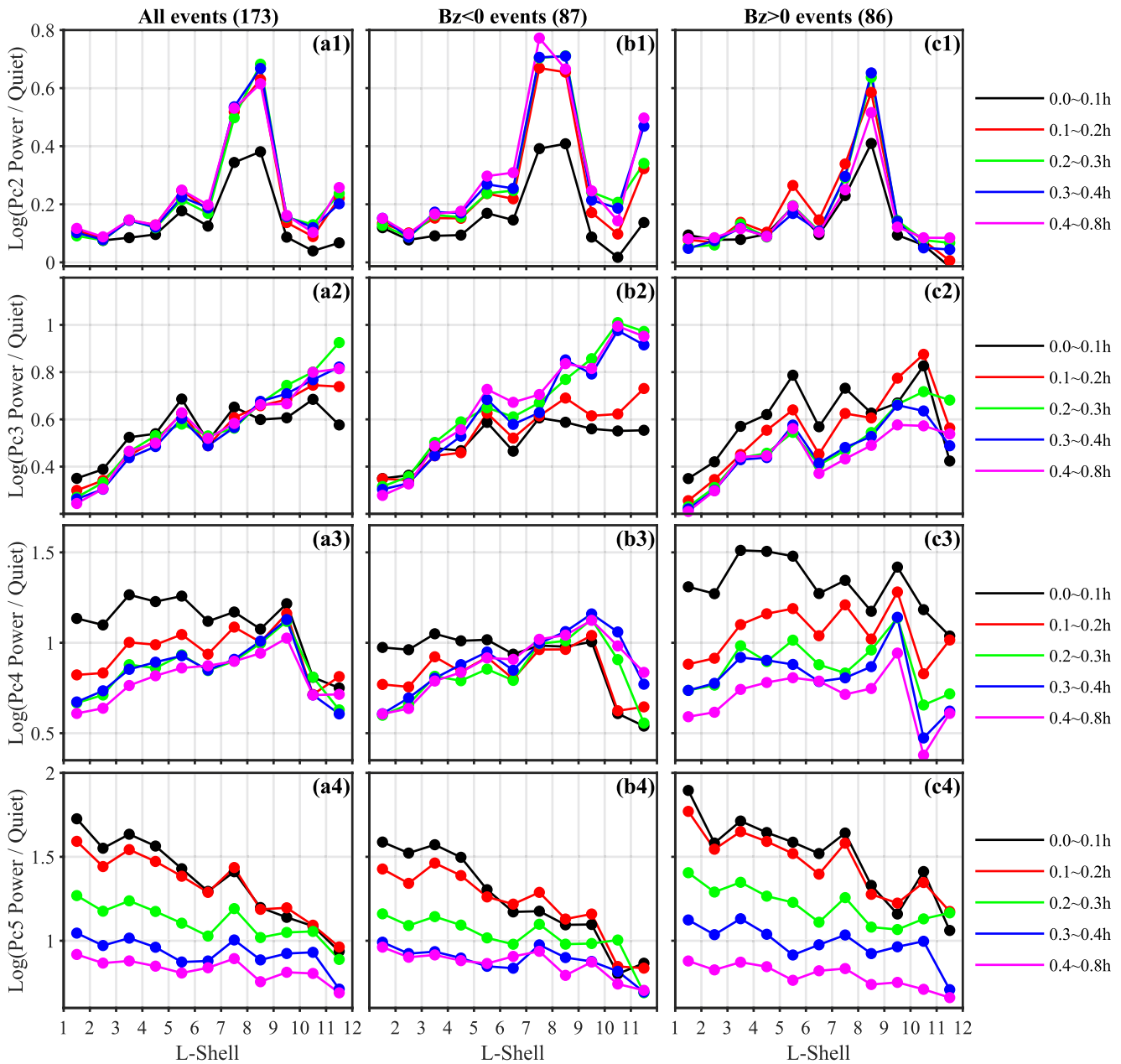


**Figure 6.** After the dynamic pressure pulses arrival, the ratio of the power relative to the quiet period at different L-shells. From left column to right column, the IMF conditions and the corresponding number of events are marked on the top of (a1–c1), respectively. Lines with different colors in each panel represent different time periods after the arrival of the dynamic pressure pulses.

pulses to the quiet period for different L-shells and frequency bands. The power enhancement in the Pc2 band is mainly concentrated from $L = 7$ to $L = 9$, as shown in Figures 6a1–6c1. The width of this region exhibits a strong dependence on the IMF Bz component. For southward IMF, the Pc2 power enhanced region width is close to one L-shell as shown in Figure 6b1. Additionally, near the magnetopause at $L > 10$, it can be observed that the Pc2 wave power enhancement triggered by dynamic pressure pulses with southward IMF increases with time, but this feature is not observed when Bz > 0.

The power enhancement ratio for the Pc3 band exhibits a downward trend from high to low L-shell. This result suggests that the Pc3 ULF waves observed on the ground originate from external sources. The Pc4 ULF waves exhibit some intriguing phenomena. For dynamic pressure pulses with southward IMF, there is a clear boundary around $L = 7$. For $L < 7$, the Pc4 wave power decays with time, whereas for $L > 7$, the power grows with time.

**Table 1**
*Characteristics of Pc2-5 Wave Power*

| | Pc2 | Pc3 | Pc4 | Pc5 |
|---|---|---|---|---|
| Decay timescale | Not clear | 6 mins | 8 mins | 15 mins |
| Enhancement ratio (inner to outer L-shell) | Maximum at $L = 7 \sim 9$ | Increases | Irregular | Decreases |

*Note*. The second row gives the decay timescales of wave power and the third row gives the features of the power ratio relative to the quiet period along L-shells.

However, when the dynamic pressure pulses carry northward IMF, the Pc4 waves decay with time at all L-shells. For low-frequency Pc5 ULF waves, the power growth ratio decreases continuously with increasing L-shell. Moreover, with the evolution of time, the proportion of growth relative to the quiet period declines at almost every L-shell, regardless of the IMF conditions.

Table 1 summarizes the timescales of ground-observed ULF wave power decay and the features of power enhancement ratio in different frequency bands.

### 3.3. Correlation Between Season and Solar Cycle With the ULF Power

Previous studies lack long-term global statistics of ground ULF fluctuations. As the last link in the sun-terrestrial environment which is closest to human production and life, it is especially necessary to study the relationship between the ground ULF fluctuation intensity and the season, as well as the solar cycle. As shown in Figures 7a and 7c, in March and May, ULF fluctuation is stronger than in other months. We also find that the average southward IMF is larger. To some extent, wave power enhancements in spring and fall may be related to the magnitude of the southward IMF. We prefer that this seasonal effect can be explained by the Russell-McPherron (R-M) effect (Russell et al., 1974). But to our surprise, the ULF wave power in various bands does not show obvious annual variation with the number of sunspots. In addition, the occurrence rate of pulse events decreases slightly as the solar activity decreases, and the ULF power decreases as well.

## 4. Discussion

In this paper, based on magnetic field observations from global geomagnetic stations from the beginning of 2012 to the end of 2019, we conducted a statistical study on temporal and spatial variations of global ULF wave power after the positive dynamic pressure pulse arrival. The effect of IMF orientation, the evolution of pulse-induced ULF waves, and ULF power's dependence on geomagnetic indices are investigated.

### 4.1. The Controlling Effect of the IMF North-South Component on ULF Fluctuations

Our study focuses on examining the impact of IMF orientation on ULF fluctuations. Specifically, we investigate the relationship between the southward IMF and the distribution of ULF waves. Our findings indicate that when IMF is southward, ULF waves are more uniformly distributed and have a higher intensity. As presented in panels b2–b3 of Figure 5, the AE index is larger during southward IMF, indicating more intense substorm activities. Moreover, panels e1–f4 of Figure 3 demonstrate that when substorm activity is stronger, the activity of ULF waves in all frequency bands is more intense, particularly on the nightside. Finally, Figures 6b1–6c2 indicate that the ULF fluctuation power gradually increases over time in the Pc2 to Pc3 bands during southward IMF. This suggests that injection particles continuously transfer their energy to the waves during these conditions.

### 4.2. Growth and Damping of ULF Waves Triggered by the Pressure Pulses

Within 1 minute after the pulse arrival, there is a significant wave power enhancement in all L-shells. Previous studies have investigated the time scale of growth and damping of ULF fluctuations. In the event reported by Zong et al. (2009), Strong Alfvén waves with a period of approximately 100–150s decay within 15 min. The time scale of the interaction between IP shocks and the magnetosphere is about 1 min (Z. Y. Liu et al., 2017), which is consistent with our statistical results. In general, from Pc3 to Pc5 bands, the higher the L-shell is, the earlier the fluctuations are observed. The time required for the lowest L-shell to observe obvious Pc3–Pc5 fluctuations is 4–6 min. The particle number density is larger in the lower L-shells, so the ULF wave interacts with particles more frequently and decays quickly. From Pc3 to Pc5 bands, the time scales of the decay are about 6, 8 and 15 min, respectively.

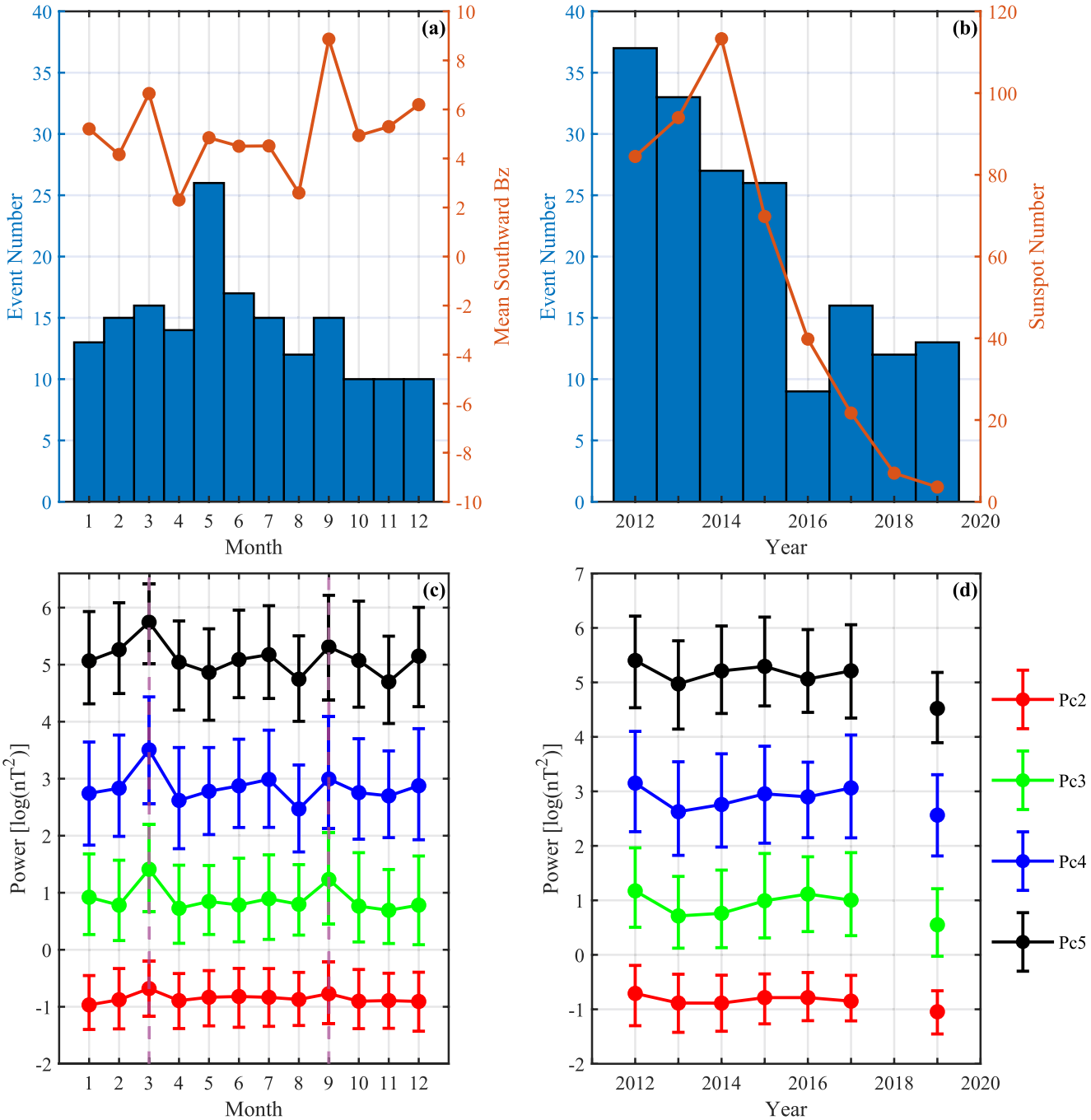


**Figure 7.** The seasonal and annual variation of power. (a) The monthly distributions of pulses events number and the average value of the southward IMF carried by the pulse for the corresponding month. (b) Yearly distributions of pulses events number and the sunspot number. (c) Power distribution of month, (d) power distribution of the year, error bars represent upper and lower quartiles.

### 4.3. Dependence of ULF Power on Kp Index, SME Index and Intensity of Pressure Change

Overall, when the Kp index during the dynamic pressure pulses is larger, the power of the ULF waves is stronger globally, consistent with previous studies (Ali et al., 2015, 2016; W. Liu et al., 2016). However, they pointed out that during events with higher Kp index, the noon portion is no longer necessarily dominant. But in our statistical results, the power of ULF waves on the dayside is significantly higher than that on the nightside, regardless of the Kp index. This is because the ULF wave activities we studied are all related to solar wind dynamic pressure pulses. High dynamic pressure pulses compress the dayside magnetosphere, accompanied by the increase of

dayside fluctuations. As the intensity of the dynamic pressure pulse increases, it is natural to see that the excited ULF waves will become stronger. This result further supports the idea that compressional disturbances at the magnetopause can indeed provide the energy to excite these waves.

Our statistical analysis indicates a significant correlation between ULF wave power and substorm activity. This correlation can be explained by the process of wave-particle interaction. The effect of this interaction is dependent on the properties of both waves and particles. Various mechanisms responsible for generating ULF waves on the nightside have been discussed by Tian et al. (2012) and Shi et al. (2013). They have reported that ULF waves can be excited in the tail plasma sheet in response to the IP shock. Furthermore, Studies conducted by Hao et al. (2014) have shown that ULF waves can accelerate substorm-injected electrons to high energies through drift resonance acceleration. Our analysis of magnetic field observations from ground-based stations provides further evidence for the close relationship between ground ULF fluctuations and substorm activity.

### 4.4. Behaviors of ULF Power at Different L-Shells

The power enhancement in the Pc2 band is mainly concentrated from $L = 7$ to $L = 9$, outside the plasmapause. The possible reason is that the magnetopause on the dayside is compressed by the pressure pulses, which increases the anisotropy of the ions, produces cyclotron instability, and leads to the growth of the Pc2 waves.

In addition, it is very interesting that the Pc3 band and the Pc5 band exhibit completely different characteristics for the ratio of the power enhancement to the calm period, which implies the different sources of these two types of waves. The Pc3-5 ULF waves observed on the ground have different sources, including K-H instability, upstream waves near the foreshock, cavity modes, and field line resonances produced by various disturbance sources inside and outside the magnetosphere, etc. Some of the Pc3 fluctuations observed on the ground are considered to be related to upstream waves. These fast mode waves can be generated by the upstream ion-cyclotron resonance mechanism and then propagate to the ground and produce Pc3 geomagnetic pulsations on the dayside (Kim et al., 1998; Takahashi et al., 2016; Troitskaya, 1971; Vellante et al., 1996). The strongest evidence for this explanation comes from the better correlation of frequency with the IMF cone angle (Le & Russell, 1994; Takahashi et al., 1984). In our statistics, it can be seen that in the foreshock area on the morning side, the power of the Pc3 band is higher than that of any surrounding areas, and the Pc3 fluctuations at high L-shells are also stronger, which implies the upstream wave origin of the Pc3 ULF fluctuations.

Observations of Pc5 band ULF fluctuations reveal that wave power at lower L-shells exhibits a significantly greater increase compared to the quiet period. This behavior can be attributed to the low L-shell region located inside the plasmapause, where sharp density gradients may affect the properties of waves propagating from the outer magnetosphere. Consequently, ULF waves observed in this region may differ from those observed in the outer magnetosphere. Previous studies have shown that fast mode waves can be trapped within the plasmasphere and subsequently coupled to local standing Alfvén waves (Allan et al., 1986; Krauss-Varban & Patel, 1988; Zhu & Kivelson, 1989). This mechanism provides a plausible explanation for the occurrence of ULF waves in the low-latitude region of the magnetosphere.

### 4.5. The R-M Effect on the ULF Power

The intensity of magnetic field fluctuations exhibits seasonal variability, with higher power levels observed in March and September. It is hypothesized that this variation may be linked to the R-M effect, which is the most commonly accepted explanation for the semi-annual variation in geomagnetic activity (Russell et al., 1974). The R-M effect regulates ULF wave power by influencing the polarity of the IMF (Zhao & Zong, 2012). Our findings provide further support for this hypothesis.

## 5. Conclusion

In this study, we have systematically studied the temporal and spatial changes of the ground-based ULF magnetic wave power in response to the arrival of positive dynamic pressure pulses under different solar wind conditions. The main results are summarized as follows:

1. The response of ground magnetic field to dynamic pressure pulses occurs within 1 minute, with ULF waves reaching their peak power at low L-shells within 4–6 min. The magnitude of the Pc3 to Pc5 waves decays in a time scale for about 6, 8, and 15 min, respectively.

2. Southward IMF during pressure impulses can trigger more intense substorm activity, accompanied by increasing wave power across various frequency bands globally.
3. Compared to quiet periods, Pc2 fluctuation enhancement primarily occurs at $L = 7$ to 9. The proportion of Pc3 enhancement is greater at high L-shells, while the opposite is true for Pc5 fluctuations, indicating different excitation and propagation mechanisms.
4. Seasonal effects significantly influence magnetic field wave power in different bands, which can be further explained by the R-M effect.

Our work provides a better understanding of the role of ULF waves in regulating solar wind-magnetospheric energy transfer, and the effect of solar wind dynamic pressure pulses on geomagnetic activity. Solar wind dynamic pressure pulses are a possible source of ULF fluctuations on the ground. This work is based on the integrated power intensity of different bands of the global geomagnetic stations, and it would be helpful to compare the results with observations of satellites in the LEO orbit, such as the SWARM (Friis-Christensen et al., 2006) and CHAMP (Reigber et al., 2002). Widespread asymmetries in different solar wind conditions need to be further studied.

## Data Availability Statement

One-second resolution ULF parameters derived from ground magnetometer measurements can be obtained from Johns Hopkins Applied Physics Laboratory (https://supermag.jhuapl.edu/). The Wind shock database can be found at https://www.cfa.harvard.edu/shocks/wi_data/. OMNI data can be obtained from the Space Physics Data Facility at the NASA Goddard Space Flight Center (https://cdaweb.gsfc.nasa.gov/index.html/).

**Acknowledgments**
We are very grateful to the entire SuperMAG team for providing high-resolution magnetic fields and ULF parameters data. The authors thank the Harvard Smithsonian Center for Astrophysics and the NASA SPDF/CDAWeb team for the interplanetary shock analysis and Wind data. This work was supported by the National Natural Science Foundation of China (42230202, 42274202) and the National Key R&D Program of China (2020YFE0202100), the Informatization Plan of Chinese Academy of Sciences (Grant CAS-WX2021PY-0101), and the Science and Technology Development Fund, Macau SAR (File no. SKL-LPS(MUST)-2021-2023).

## References

Ali, A. F., Elkington, S. R., Tu, W., Ozeke, L. G., Chan, A. A., & Friedel, R. H. W. (2015). Magnetic field power spectra and magnetic radial diffusion coefficients using CRRES magnetometer data. *Journal of Geophysical Research: Space Physics*, *120*(2), 973–995. https://doi.org/10.1002/2014ja020419

Ali, A. F., Malaspina, D. M., Elkington, S. R., Jaynes, A. N., Chan, A. A., Wygant, J., & Kletzing, C. A. (2016). Electric and magnetic radial diffusion coefficients using the Van Allen probes data. *Journal of Geophysical Research: Space Physics*, *121*(10), 9586–9607. https://doi.org/10.1002/2016ja023002

Allan, W., Poulter, E. M., & White, S. P. (1986). Hydromagnetic wave coupling in the magnetosphere? Plasmapause effects on impulse-excited resonances. *Planetary and Space Science*, *34*(12), 1189–1200. https://doi.org/10.1016/0032-0633(86)90056-5

Allen, R. C., Zhang, J. C., Kistler, L. M., Spence, H. E., Lin, R. L., Klecker, B., et al. (2015). A statistical study of EMIC waves observed by cluster: 1. Wave properties. *Journal of Geophysical Research: Space Physics*, *120*(7), 5574–5592. https://doi.org/10.1002/2015ja021333

Anderson, B. J., Engebretson, M. J., Rounds, S. P., Zanetti, L. J., & Potemra, T. A. (1990). A statistical study of Pc 3--5 pulsations observed by the AMPTE/CCE magnetic fields experiment, 1. Occurrence distributions. *Journal of Geophysical Research*, *95*(A7), 10495–10523. https://doi.org/10.1029/ja095ia07p10495

Anderson, B. J., Erlandson, R. E., & Zanetti, L. J. (1992). A statistical study of Pc 1--2 magnetic pulsations in the equatorial magnetosphere: 1. Equatorial occurrence distributions. *Journal of Geophysical Research*, *97*(A3), 3075–3088. https://doi.org/10.1029/91ja02706

Anderson, B. J., & Hamilton, D. C. (1993). Electromagnetic ion cyclotron waves stimulated by modest magnetospheric compressions. *Journal of Geophysical Research*, *98*(A7), 11369–11382. https://doi.org/10.1029/93ja00605

Angelopoulos, V. (2008). The THEMIS mission. *Space Science Reviews*, *141*(1–4), 5–34. https://doi.org/10.1007/s11214-008-9336-1

Baker, G. J., Donovan, E. F., & Jackel, B. J. (2003). A comprehensive survey of auroral latitude Pc5 pulsation characteristics. *Journal of Geophysical Research*, *108*(A10), 1384. https://doi.org/10.1029/2002ja009801

Chapman, S., & Bartels, J. (1940). *Geomagnetism, vol. II: Analysis of the data, and physical theories*. Geomagnetism.

Engebretson, M. J., Posch, J. L., Wygant, J. R., Kletzing, C. A., Lessard, M. R., Huang, C., et al. (2015). Van Allen probes, NOAA, GOES, and ground observations of an intense EMIC wave event extending over 12 h in magnetic local time. *Journal of Geophysical Research: Space Physics*, *120*(7), 5465–5488. https://doi.org/10.1002/2015ja021227

Friis-Christensen, E., Lühr, H., & Hulot, G. (2006). Swarm: A constellation to study the Earth's magnetic field. *Earth Planets and Space*, *58*(4), 351–358. https://doi.org/10.1186/bf03351933

Gjerloev, J. W. (2012). The SuperMAG data processing technique. *Journal of Geophysical Research*, *117*(A9), A09213. https://doi.org/10.1029/2012ja017683

Greenstadt, E. W., & Russell, C. T. (1994). *Stimulation of exogenic, daytime geomagnetic pulsations: A global perspective* (Vol. 81, pp. 13–23). Washington DC American Geophysical Union Geophysical Monograph Series.

Hao, Y. X., Zong, Q., Wang, Y. F., Zhou, X., Zhang, H., Fu, S. Y., et al. (2014). Interactions of energetic electrons with ULF waves triggered by interplanetary shock: Van Allen Probes observations in the magnetotail. *Journal of Geophysical Research*, *119*(10), 8262–8273. https://doi.org/10.1002/2014JA020023

Hao, Y. X., Zong, Q. G., Zhou, X. Z., Rankin, R., Chen, X. R., Liu, Y., et al. (2019). Global-scale ULF waves associated with SSC accelerate magnetospheric ultrarelativistic electrons. *Journal of Geophysical Research: Space Physics*, *124*(3), 1525–1538. https://doi.org/10.1029/2018ja026134

Hao, Y. X., Zong, Q. G., Zhou, X. Z., Rankin, R., Chen, X. R., Liu, Y., et al. (2017). Relativistic electron dynamics produced by azimuthally localized poloidal mode ULF waves: Boomerang-shaped pitch angle evolutions. *Geophysical Research Letters*, *44*(15), 7618–7627. https://doi.org/10.1002/2017GL074006

Jacobs, J. A., Kato, Y., Matsushita, S., & Troitskaya, V. A. (1964). Classification of geomagnetic micropulsations. *Journal of Geophysical Research*, *69*(1), 180–181. https://doi.org/10.1029/JZ069i001p00180

Jun, C.-W., Miyoshi, Y., Kurita, S., Yue, C., Bortnik, J., Lyons, L., et al. (2021). The characteristics of EMIC waves in the magnetosphere based on the Van Allen Probes and Arase observations. *Journal of Geophysical Research: Space Physics*, *126*(6), e2020JA029001. https://doi.org/10.1029/2020ja029001

Kim, K.-H., Takahashi, K., & Anderson, B. J. (1998). Ground-satellite coherence analysis of Pc3 pulsations. *Journal of Geophysical Research*, *103*(A6), 11755–11769. https://doi.org/10.1029/98ja00617

King, J. H., & Papitashvili, N. E. (2005). Solar wind spatial scales in and comparisons of hourly wind and ACE plasma and magnetic field data. *Journal of Geophysical Research*, *110*(A2), A02104. https://doi.org/10.1029/2004ja010649

Krauss-Varban, D., & Patel, V. L. (1988). Numerical analysis of the coupled hydromagnetic wave equations in the magnetosphere. *Journal of Geophysical Research*, *93*(A9), 9721–9729. https://doi.org/10.1029/ja093ia09p09721

Le, G., & Russell, C. T. (1994). *The morphology of ULF waves in the Earth's foreshock* (Vol. 81, pp. 87–98). Washington DC American Geophysical Union Geophysical Monograph Series.

Lepping, R. P., Acūna, M. H., Burlaga, L. F., Farrell, W. M., Slavin, J. A., Schatten, K. H., et al. (1995). The WIND magnetic field investigation. *Space Science Reviews*, *71*(1–4), 207–229. https://doi.org/10.1007/BF00751330

Li, X., Baker, D. N., Elkington, S., Temerin, M., Reeves, G. D., Belian, R. D., et al. (2003). Energetic particle injections in the inner magnetosphere as a response to an interplanetary shock. *Journal of Atmospheric and Solar-Terrestrial Physics*, *65*(2), 233–244. https://doi.org/10.1016/S1364-6826(02)00286-9

Lin, R. P., Anderson, K. A., Ashford, S., Carlson, C., Curtis, D., Ergun, R., et al. (1995). A three-dimensional plasma and energetic particle investigation for the Wind spacecraft. *Space Science Reviews*, *71*(1–4), 125–153. https://doi.org/10.1007/bf00751328

Liu, W., Sarris, T. E., Li, X., Elkington, S. R., Ergun, R., Angelopoulos, V., et al. (2009). Electric and magnetic field observations of Pc4 and Pc5 pulsations in the inner magnetosphere: A statistical study. *Journal of Geophysical Research*, *114*(A12), A12206. https://doi.org/10.1029/2009JA014243

Liu, W., Tu, W., Li, X., Sarris, T., Khotyaintsev, Y., Fu, H., et al. (2016). On the calculation of electric diffusion coefficient of radiation belt electrons with in situ electric field measurements by THEMIS. *Geophysical Research Letters*, *43*(3), 1023–1030. https://doi.org/10.1002/2015gl067398

Liu, Y., & Zong, Q. G. (2015). Energetic electron response to interplanetary shocks at geosynchronous orbit. *Journal of Geophysical Research*, *120*(6), 4669–4683. https://doi.org/10.1002/2014JA020756

Liu, Z. Y., Zong, Q. G., Hao, Y. X., Zhou, X. Z., Ma, X. H., & Liu, Y. (2017). Electron dropout echoes induced by interplanetary shock: A statistical study. *Journal of Geophysical Research*, *122*(8), 8037–8050. https://doi.org/10.1002/2017JA024045

Liu, Z. Y., Zong, Q. G., Rankin, R., Zhang, H., Wang, Y. F., Zhou, X. Z., et al. (2022). Simultaneous macroscale and microscale wave–ion interaction in near-earth space plasmas. *Nature Communications*, *13*(1), 5593. https://doi.org/10.1038/s41467-022-33298-6

Liu, Z. Y., Zong, Q. G., Zhou, X. Z., Zhu, Y. F., & Gu, S. J. (2020). Pitch angle structures of ring current ions induced by evolving poloidal ultra-low frequency waves. *Geophysical Research Letters*, *47*(4), e2020GL087203. https://doi.org/10.1029/2020GL087203

Min, K., Lee, J., Keika, K., & Li, W. (2012). Global distribution of EMIC waves derived from THEMIS observations. *Journal of Geophysical Research*, *117*(A5), A05219. https://doi.org/10.1029/2012ja017515

Potemra, T. A., Zanetti, L. J., & Acuna, M. H. (1985). The AMPTE CCE magnetic field experiment. *IEEE Transactions on Geoscience and Remote Sensing*(3), 246–249. https://doi.org/10.1109/tgrs.1985.289521

Reigber, C., Lühr, H., & Schwintzer, P. (2002). CHAMP mission status. *Advances in Space Research*, *30*(2), 129–134. https://doi.org/10.1016/s0273-1177(02)00276-4

Ren, J., Zong, Q. G., Wang, Y. F., & Zhou, X. Z. (2015). The interaction between ULF waves and thermal plasma ions at the plasmaspheric boundary layer during substorm activity. *Journal of Geophysical Research: Space Physics*, *120*(2), 1133–1143. https://doi.org/10.1002/2014ja020766

Russell, C. T., McPherron, R. L., & Burton, R. K. (1974). On the cause of geomagnetic storms. *Journal of Geophysical Research*, *79*(7), 1105–1109. https://doi.org/10.1029/ja079i007p01105

Shi, Q. Q., Hartinger, M., Angelopoulos, V., Zong, Q. G., Zhou, X. Z., Zhou, X. Y., et al. (2013). THEMIS observations of ULF wave excitation in the nightside plasma sheet during sudden impulse events. *Journal of Geophysical Research: Space Physics*, *118*(1), 284–298. https://doi.org/10.1029/2012ja017984

Takahashi, K., & Anderson, B. J. (1992). Distribution of ULF energy ($f$<80 mHz) in the inner magnetosphere: A statistical analysis of AMPTE CCE magnetic field data. *Journal of Geophysical Research*, *97*(A7), 10751–10773. https://doi.org/10.1029/92ja00328

Takahashi, K., Hartinger, M. D., Malaspina, D. M., Smith, C. W., Koga, K., Singer, H. J., et al. (2016). Propagation of ULF waves from the upstream region to the midnight sector of the inner magnetosphere. *Journal of Geophysical Research: Space Physics*, *121*(9), 8428–8447. https://doi.org/10.1002/2016ja022958

Takahashi, K., McPherron, R. L., & Terasawa, T. (1984). Dependence of the spectrum of Pc 3--4 pulsations on the interplanetary magnetic field. *Journal of Geophysical Research*, *89*(A5), 2770–2780. https://doi.org/10.1029/ja089ia05p02770

Tan, L. C., Fung, S. F., & Shao, X. (2004). Observation of magnetospheric relativistic electrons accelerated by Pc-5 ULF waves. *Geophysical Research Letters*, *31*(14), L14802. https://doi.org/10.1029/2004gl019459

Tian, A. M., Zong, Q. G., Zhang, T. L., Nakamura, R., Du, A. M., Baumjohann, W., et al. (2012). Dynamics of long-period ULF waves in the plasma sheet: Coordinated space and ground observations. *Journal of Geophysical Research*, *117*(A3), A03211. https://doi.org/10.1029/2011ja016551

Troitskaya, V. A. (1971). *Relationship between Pc 2-4 pulsation and interplanetary field*, In D. Akad, & USSR Nauk (Eds.), (Eds). (p. 1312).

Usanova, M. E., Mann, I. R., Rae, I. J., Kale, Z. C., Angelopoulos, V., Bonnell, J. W., et al. (2008). Multipoint observations of magnetospheric compression-related EMIC Pc1 waves by THEMIS and CARISMA. *Geophysical Research Letters*, *35*(17), L17S25. https://doi.org/10.1029/2008gl034458

Vassiliadis, D., Mann, I. R., Fung, S. F., & Shao, X. (2007). Ground Pc3--Pc5 wave power distribution and response to solar wind velocity variations. *Planetary and Space Science*, *55*(6), 743–754. https://doi.org/10.1016/j.pss.2006.03.012

Vellante, M., Villante, U., De Lauretis, M., & Barchi, G. (1996). Solar cycle variation of the dominant frequencies of Pc3 geomagnetic pulsations at L=1.6. *Geophysical Research Letters*, *23*(12), 1505–1508. https://doi.org/10.1029/96gl01399

Yan, Y., Yue, C., Ma, Q., Zhou, X.-Z., Zong, Q.-G., Fu, H., et al. (2023). Prompt appearance of large-amplitude EMIC waves induced by solar wind dynamic pressure enhancement and the subsequent relativistic electron precipitation. *Journal of Geophysical Research: Space Physics*, *128*(7), e2023JA031399. https://doi.org/10.1029/2023JA031399

Yan, Y., Yue, C., Yin, Z.-F., Zhou, X.-Z., Zong, Q.-G., & Li, J.-H. (2023). Amplitude-dependent properties and excitation mechanisms of EMIC waves in the Earth's Inner magnetosphere. *Journal of Geophysical Research: Space Physics*, *128*(7), e2023JA031451. https://doi.org/10.1029/2023JA031451

Yang, B., Fu, S., Zong, Q., Wang, Y., Zhou, X., Pu, Z., & Xie, L. (2008). Numerical study on ULF waves in a dipole field excited by sudden impulse. *Science in China - Series E: Technological Sciences*, *51*(10), 1665–1676. https://doi.org/10.1007/s11431-008-0251-1

Yue, C., Li, W., Nishimura, Y., Zong, Q., Ma, Q., Bortnik, J., et al. (2016). Rapid enhancement of low-energy (<100 eV) ion flux in response to interplanetary shocks based on two Van Allen Probes case studies: Implications for source regions and heating mechanisms. *Journal of Geophysical Research*, *121*(7), 6430–6443. https://doi.org/10.1002/2016JA022808

Yue, C., Zong, Q., Wang, Y., Vogiatzis, I. I., Pu, Z., Fu, S., & Shi, Q. (2011). Inner magnetosphere plasma characteristics in response to interplanetary shock impacts. *Journal of Geophysical Research*, *116*(A11), A11206. https://doi.org/10.1029/2011ja016736

Yue, C., Zong, Q. G., Zhang, H., Wang, Y. F., Yuan, C. J., Pu, Z. Y., et al. (2010). Geomagnetic activity triggered by interplanetary shocks. *Journal of Geophysical Research*, *115*(A5), A00I05. https://doi.org/10.1029/2010ja015356

Zhang, X., Zong, Q., Yang, B., & Wang, Y. (2009). Numerical simulation of magnetospheric ULF waves excited by positive and negative impulses of solar wind dynamic pressure. *Science in China - Series E: Technological Sciences*, *52*(10), 2886–2894. https://doi.org/10.1007/s11431-009-0270-6

Zhang, X. Y., Zong, Q. G., Wang, Y. F., Zhang, H., Xie, L., Fu, S. Y., et al. (2010). ULF waves excited by negative/positive solar wind dynamic pressure impulses at geosynchronous orbit. *Journal of Geophysical Research*, *115*(A10), A10221. https://doi.org/10.1029/2009JA015016

Zhao, H., & Zong, Q. G. (2012). Seasonal and diurnal variation of geomagnetic activity: Russell-McPherron effect during different IMF polarity and/or extreme solar wind conditions. *Journal of Geophysical Research*, *117*(A11), A11222. https://doi.org/10.1029/2012ja017845

Zhu, X., & Kivelson, M. G. (1989). Global mode ULF pulsations in a magnetosphere with a nonmonotonic Alfvén velocity profile. *Journal of Geophysical Research*, *94*(A2), 1479–1485. https://doi.org/10.1029/JA094iA02p01479

Zong, Q. G., Rankin, R., & Zhou, X. Z. (2017). The interaction of ultra-low-frequency pc3-5 waves with charged particles in Earth's magnetosphere. *Reviews of Modern Plasma Physics*, *1*(10), 10. https://doi.org/10.1007/s41614-017-0011-4

Zong, Q. G., Wang, Y. F., Zhang, H., Fu, S. Y., Zhang, H., Wang, C. R., et al. (2012). Fast acceleration of inner magnetospheric hydrogen and oxygen ions by shock induced ULF waves. *Journal of Geophysical Research*, *117*(A11), A11206. https://doi.org/10.1029/2012JA018024

Zong, Q. G., Zhou, X. Z., Wang, Y. F., Li, X., Song, P., Baker, D. N., et al. (2009). Energetic electrons response to ULF waves induced by interplanetary shocks in the outer radiation belt. *Journal of Geophysical Research*, *114*(A10), A10204. https://doi.org/10.1029/2009JA014393